

## CHAPTER 3

# Synthesis of $\alpha$ -Fe<sub>2</sub>O<sub>3</sub> nanopowder by using Oxalate precursor based method

### 3.1 Experimental Procedure for Chemical Synthesis:

The starting chemicals used were ferric nitrate nonahydrate (99.9%, Merck, India) and oxalic acid dihydrate (99.9%, Merck, India) without further purification.

Aqueous solutions of oxalic acid and ferric nitrate were mixed in a molar ratio of 3:1 and stirred for 1 hour at room temperature using a magnetic stirrer. A greenish yellow colored precursor was formed when this mixture was evaporated on a hot plate at  $\sim 125^{\circ}\text{C}$ . Further drying for about 1 hour changed the color of the precursor to dark brown.

Iron oxide powder was prepared by grinding this dark brown precursor powder followed by calcination in air for two and a half hours at different temperatures ranging from 250 -  $450^{\circ}\text{C}$  [124, 129]. In order to avoid contamination of the precursor by carbon, a few drops of saturated ammonium nitrate solution was added to the precursor powders during the time of calcination.

### 3.2 Results and Discussion:

#### 3.2.1 Thermal Analysis:

The TG, DTG, and DSC thermograms of the precursor in air are shown in Fig 3.1.

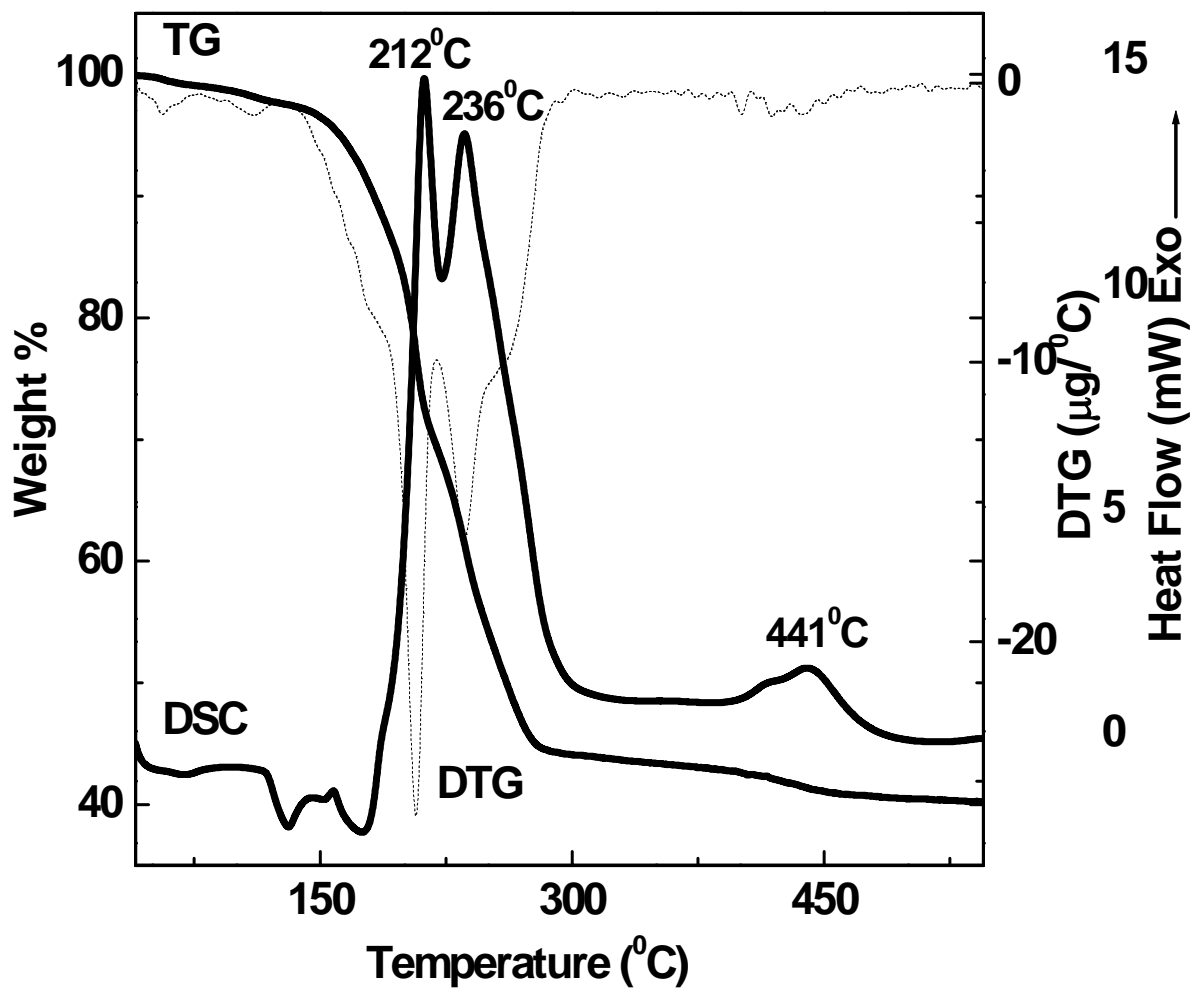


Fig.3.1 TG-DTG and DSC thermograms of the precursor in air.

The main features of the thermograms are as follows:

- (i) In TG thermogram, a total weight loss of ~ 60% occurred due to thermal decomposition of the precursor.
- (ii) About 10% of this weight loss occurred in the temperature range of 40-190<sup>0</sup>C. It was due to elimination of moisture from surface of sample, followed by strongly bound water molecules. Elimination of these H<sub>2</sub>O molecules was reflected in DSC thermogram as endothermic peaks at 130 and 174<sup>0</sup>C respectively.
- (iii) Major weight loss of ~50% was observed in the region of 190 to 450<sup>0</sup>C. This was due to the oxidative decomposition of precursor, accompanied by the evolution of CO<sub>2</sub> and NO<sub>x</sub> gases. This decomposition was observed in DSC thermogram as exothermic peaks at 212, 236<sup>0</sup>C and 441<sup>0</sup>C.
- (iv) Heating the sample beyond 450<sup>0</sup>C resulted in neither a weight loss nor formation of any new peak in DSC thermogram. It, therefore, confirmed the full decomposition of the precursor to iron oxide at ~450<sup>0</sup>C [124, 129].

### 3.2.2 X-Ray Analysis:

Room temperature XRD spectra of precursor powders at different calcination temperatures are shown in Fig. 3.2. The important features of the XRD spectra are as follows:

- (i) Appearance of two main intensity peaks corresponding to (104) and (110) diffraction planes for precursor as well as for powder calcined at 250<sup>0</sup>C, indicated the beginning of the formation of  $\alpha$ -Fe<sub>2</sub>O<sub>3</sub> phase.
- (ii) Complete formation of single phase  $\alpha$ -Fe<sub>2</sub>O<sub>3</sub> occurred when precursor was calcined at 450<sup>0</sup>C for two and a half hours in air [124, 129]. Appearance of diffraction peaks at  $2\theta = 24.4^{\circ}$ ,  $33.3^{\circ}$ ,  $35.8^{\circ}$ ,  $41.0^{\circ}$ ,  $49.5^{\circ}$ ,  $54.3^{\circ}$ ,  $57.7^{\circ}$ ,  $62.6^{\circ}$ , and  $64.2^{\circ}$  were in good agreement with the corresponding (012), (104), (110), (113), (024), (116), (018), (214) and (300) diffraction planes of  $\alpha$ -Fe<sub>2</sub>O<sub>3</sub> respectively (JCPDS 80-2377).
- (iii) Slow scan of the two main intensity peaks was performed and crystallite size of powders calcined at different temperatures was calculated using Scherrer's equation [125]. They lie in the range of 10-30 nm depending upon the calcination temperature.

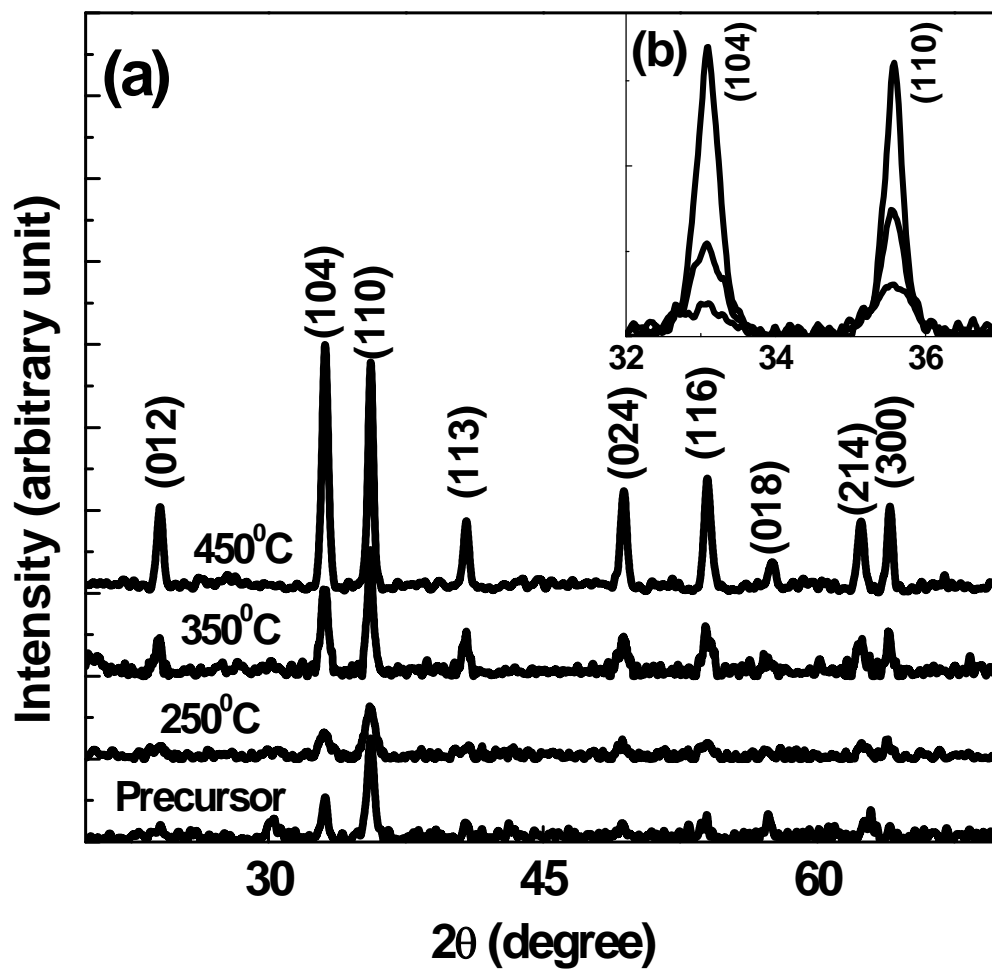


Fig 3.2 (a) X-ray diffraction spectra of precursor powders at different calcination temperatures (b) slow scan of the (104) and (110) diffraction planes.

### **3.2.3 TEM Analysis:**

TEM micrograph of the powder calcined at 450<sup>0</sup>C is shown in Fig. 3.3. It clearly indicated that average particle size of the calcined powders is ~25 nm and it matched well with that calculated by using XRD analysis. The particles were mostly elongated in shape and formed loose aggregates.

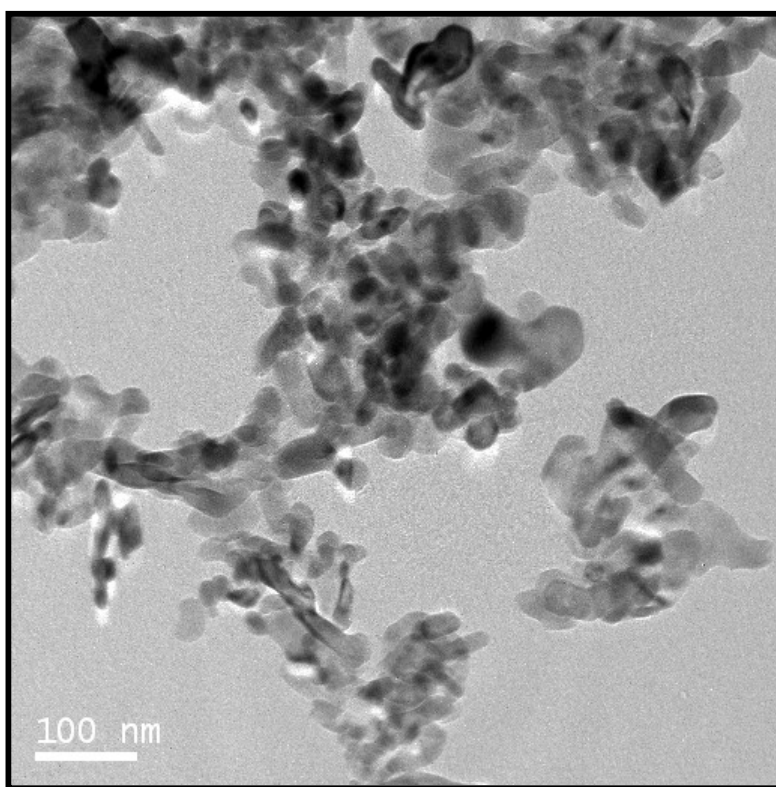


Fig 3.3 TEM micrograph of  $\alpha$ -Fe<sub>2</sub>O<sub>3</sub> powder calcined at 450<sup>0</sup>C.

### 3.2.4 SEM Analysis:

The SEM study was performed by preparing two kinds of samples. One sample was the calcined precursor that constituted of nanosized grains and the other was obtained by sintering the as-obtained nanopowder at a temperature of 1100<sup>0</sup>C for 2 hours. The SEM micrographs are shown in Fig. 3.4(a) and (b).

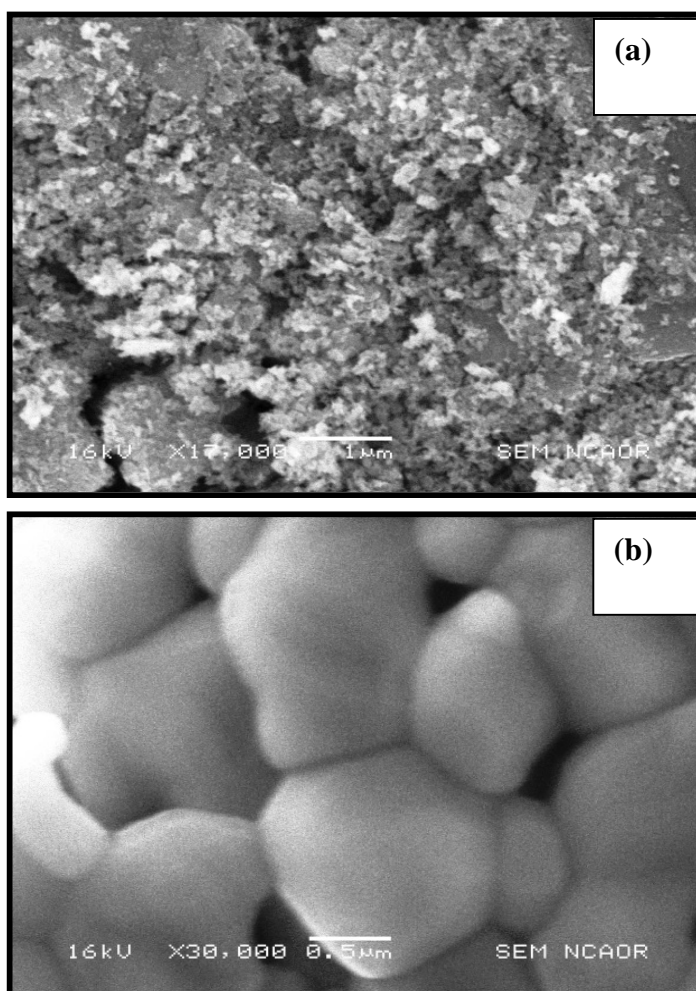


Fig. 3.4 SEM micrographs of  $\alpha$ -Fe<sub>2</sub>O<sub>3</sub> powder (a) calcined at 450<sup>0</sup>C (b) sintered at 1100<sup>0</sup>C.

The micrographs exhibited the following features:

- (i) The unsintered nanopowder formed loose aggregates of nanoparticles and high amount of porosity was observed.
- (ii) Sintering the nanoparticles at high temperature resulted in a uniformly distributed microstructure constituting of micron-sized grains. Coarsening of grains at elevated temperature was observed due to fusion of the nanosize particles.
- (iii) The particles in both cases were found to be elongated and the shape of particles was in *sync* with the hexagonal corundum structure of  $\alpha$ -Fe<sub>2</sub>O<sub>3</sub> [1].

### 3.2.5 DC resistivity measurement:

The variation of resistivity with change in temperature was studied for two cases (i) unsintered pellet and (ii) pellet sintered at 1100<sup>0</sup>C and these are shown in Fig. 3.5(a) and (b). Room temperature recorded was 25<sup>0</sup>C. The green density and sintered density of the pellets was calculated by using the dimensions of the pellets.

Case (i) unsintered pellet:

It was observed that the DC resistivity behaviour of the unsintered sample was affected by the presence of moisture in the air (moisture recorded in our lab was ~91%). As seen in SEM micrograph (Fig. 3.4(a)), the microstructure of the unsintered sample consisted of loosely agglomerated particles with high intergranular porosity (green density was ~ 2.5 g/cm<sup>3</sup>). The adsorption of moisture in the nanopores and the subsequent elimination of moisture at ~100<sup>0</sup>C led to the maximum in the resistivity [12, 13, 123, 126]. Beyond ~100<sup>0</sup>C, when all moisture was eliminated, the curve exhibited the typical NTCR (negative temperature coefficient of resistance) behavior of bulk hematite [127].

Case (ii) pellet sintered at 1100<sup>0</sup>C:

The sintered sample attained a densification of ~ 4.1 g/cm<sup>3</sup> which was lower than that obtained in case of PVA precursor based method. The resistivity behavior for the sintered sample was affected by the presence of humidity. However, the effect of moisture in the resistivity behavior

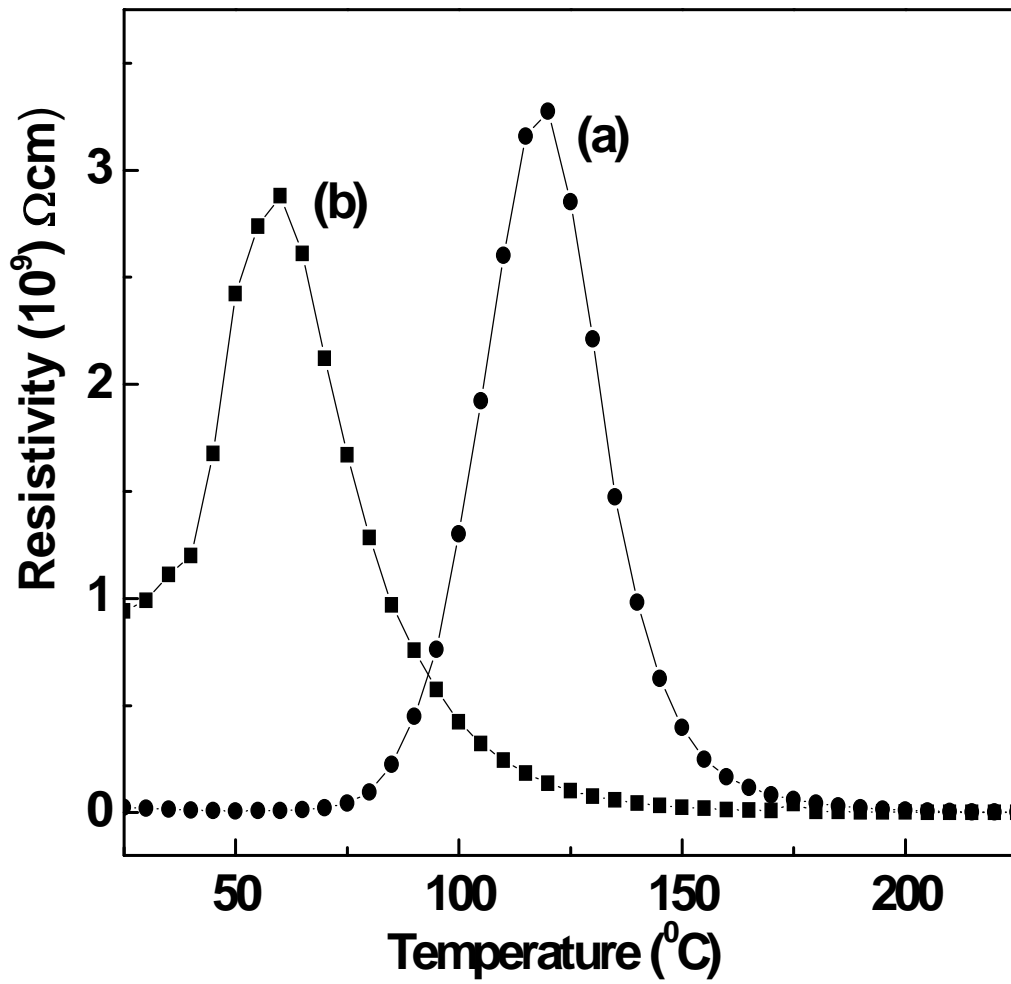


Fig. 3.5 Variation of DC resistivity with change in temperature of  $\alpha\text{-Fe}_2\text{O}_3$  powder for (a) unsintered sample (b) sample sintered at  $1100^\circ\text{C}$ .



was less pronounced as compared to that of the as-synthesized nanopowder. The elimination of moisture in this case occurred at a lower temperature  $\sim 60^{\circ}\text{C}$ . This was due to elimination of moisture from fewer numbers of pores as compared to those present in the unsintered nanopowder. Microstructure observed in SEM micrograph (Fig. 3.4(b)) of the sintered sample supported its resistivity behavior.

### **Discussion:**

TG-DTG-DSC, XRD and TEM analyses of the synthesized precursors and calcined powders confirmed that oxidative decomposition of precursor leads to the formation of single phase  $\alpha$ -Fe<sub>2</sub>O<sub>3</sub> nanopowders. In this chemical method, the reaction of oxalic acid with ferric nitrate results in formation of iron oxalate chelate complex. The chelating agent (oxalic acid) is used to keep the metal ions homogeneously dispersed in the aqueous solution. Complete dehydration of this solution is accompanied by the partial decomposition of the iron oxalate chelate complex and results in an organic based, voluminous mass, known as “precursor”. The thermal decomposition of the precursor causes evolution of CO<sub>2</sub> and NO<sub>x</sub> gas and formation of fine particles of iron oxide. The chelate complex nature of the precursor and *in situ* gas evolution during its decomposition prevents the agglomeration of resulting oxide particles and facilitates their nanostructure formation [57].

SEM micrographs and DC resistivity measurements indicate that the resistivity behavior with respect to temperature of the synthesized nanopowders as well as sintered sample (although less pronounced) is affected by the presence of moisture in the air due to high porosity in the samples. This indicates a correlation between the microstructure and DC resistivity measurement for the powder synthesized by oxalate precursor based method [124, 129].

### **3.3 Summary of Results:**

1.  $\alpha$ -Fe<sub>2</sub>O<sub>3</sub> nanopowder was successfully synthesized by using oxalate precursor based synthesis route.
2. Thermal decomposition of the precursor was complete at  $\sim 460^{\circ}\text{C}$ .
3. Single phase  $\alpha$ -Fe<sub>2</sub>O<sub>3</sub> was formed at a calcination temperature of  $450^{\circ}\text{C}$  for two and a half hours. in air.

4. Average particle size of the nanopowder was ~25 nm.
5. Surface morphology studies revealed that the particles were elongated in shape for nanopowders as well as sintered samples.
6. The room temperature resistivity of as-synthesized nanopowder was  $\sim 10^7 \Omega \text{ cm}$ .